

CHAPTER 3

PIC SIMULATION OF GYROKLYSTRON AMPLIFIERS*

- 3.1 Introduction
- 3.2 PIC Simulation Code 'MAGIC'
 - 3.2.1 Basics of MAGIC software
 - 3.2.2 PIC simulation description
- 3.3 PIC Simulation of a Two-Cavity Gyroklystron Amplifier
 - 3.3.1 RF interaction structure modeling
 - 3.3.2 Eigenmode and electromagnetic fields
 - 3.3.3 Electron beam and RF wave interaction
- 3.4 PIC Simulation of a Four-Cavity Gyroklystron Amplifier
 - 3.4.1 RF interaction structure modeling
 - 3.4.2 Eigenmode and electromagnetic fields
 - 3.4.3 Electron beam and RF wave interaction
- 3.5 Conclusion

*Part of this work has been published as

1. **M. S. Chauhan**, M. V. Swati and P. K. Jain, "PIC simulation study of a 35 GHz, 200 kW gyroklystron," *Journal of Microwaves, Optoelectronics and Electromagnetic Applications*, Vol. 12, No. 2, pp. 116-125, 2013.

3.1 Introduction

The electron beam and RF wave interaction mechanism in a gyrokystron amplifier is quite complex as there are a number of parameters, factors and issues, which will simultaneously affects the overall performance of the device. Therefore, in the preceding chapter, Chapter 2, the linear and nonlinear analyses of gyrokystron amplifier have been carried out to model the beam-wave interaction behavior of the device. The nonlinear analysis is capable to exhibit the large signal behavior of the gyrokystron amplifier. Due to the inherent benefits such as, applicability to variety of interaction structure, and the inclusion of inhomogeneous magnetic field, this theory has been taken up in the present thesis for analysis of the gyrokystron amplifier. Based on these analyses, computer codes have been developed and their validity has been established by comparing the numerical values thus obtained with the reported experimental results.

The beam-wave interaction behavior of the gyrokystron amplifiers have been studied through the analytical models as well as using simulation methods [Tran *et al.* (1986), Salop *et al.* (1986), Choi (1998), Geng *et al.* (2004), Luo *et al.* (2005), Wang *et al.* (2008), Lei (2009), Jianhua *et al.* (2011), Xu *et al.* (2012)]. With the advent of high speed computers, simulation and modeling techniques have been widely used for the design and performance evaluation of the device. These simulation techniques offer useful insight in understanding device behavior as well as supporting the analytical models. Particle-in-cell (PIC) simulation method is found to be useful and handy to investigate the beam-wave interaction behavior of the gyro-devices and also to optimize their performance. Both 2D and 3D PIC simulation codes, like, CHIPIC, MAGIC 2D are used for gyrokystrons in past [Choi (1998), Zhou *et al.* (2008)]. Choi (1998) used 2D MAGIC code for designing a 28 GHz, 200 kW five-cavity gyrokystron amplifier. Wang *et al.* utilized the PIC simulation technique for investigating the beam-wave interaction behavior of TE_{021} mode four-cavity gyrokystron amplifier [Wang *et al.* (2008)]. Lei designed the four-cavity 30 GHz gyrokystron amplifier through optimization of various parameters using PIC simulation [Lei (2009)]. Xu *et al.* used the PIC

simulation for validating their self-consistent theory results obtained for W-band four-cavity gyroklystron amplifier [Xu *et al.* (2012)].

In most of the reported work on the RF behavior study of the gyroklystron amplifiers, the PIC simulation technique is merely used to validate the theoretical outcomes. The complete description of the RF behavior through the PIC simulation model for a gyroklystron amplifier is not presented. In the present work, the electron beam and RF wave interaction behavior study of the typically selected 35 GHz, 200 kW two-cavity and four-cavity gyroklystron amplifiers is described in detail outlining the various steps used during the PIC simulation. Here, we have used a commercially available 3D PIC simulation code ‘MAGIC’ for this purpose. The benefits of using a 3D PIC code is that it comprehensively depicts the device geometry along with the nonlinear beam-wave interaction mechanism taking place inside the tube. Here, the beam-absent, eigenmode analysis as well as the beam present device behavior of a gyroklystron has been studied. Eigenmode analysis is carried out in the absence of electron beam using eigenmode solver to ensure the device operation in the desired mode and frequency. The exact operating mode is confirmed by observing electric and magnetic fields patterns and their variations along radial as well as axial directions. Further, electron beam present analysis is performed for the performance evaluation of the gyroklystron amplifier in all respects. The obtained results have been also verified through nonlinear analysis results obtained in previous chapter, Chapter 2, which shows agreement within ~5%.

3.2 PIC Simulation Code ‘MAGIC’

MAGIC is an electromagnetic particle-in-cell finite-difference, time-domain (EM PIC FDTD) software used for the modeling and simulation of beam wave interactions between space charge and electromagnetic fields [MAGIC user’s manual (2007)]. It simulates the interaction between charged particles and electromagnetic fields as they evolve in time and space from some defined initial configuration. The electromagnetic fields are obtained by the solution of the full set of Maxwell’s time-dependent equations. Similarly, the complete Lorentz force

equation is solved to obtain relativistic particle trajectories, and the continuity equation is solved to provide current and charge densities for Maxwell's equations. This approach, commonly referred to as electromagnetic particle-in-cell (PIC), provides self-consistent interaction between charged particles and electromagnetic fields. In addition, the code has been provided with powerful algorithms to represent structural geometries, material properties, incoming and outgoing waves, particle emission processes, and so forth. This versatility of the MAGIC code makes it suitable for the simulation of gyrokystron amplifier.

3.2.1 Basics of MAGIC software

MAGIC is a user-configurable FDTD-PIC simulation code and based on a discrete formulation of the conventional Maxwell equations. One choice for this discrete foundation begins with the “Yee Cell”. The essential properties of the “Yee Cell” formulation is that the full-grid and half-grid placement of field elements, results in perfect curl-grad = 0 and divcurl=0, in the finite difference representation. The full grid and half grid assignments are shown in Fig. 3.1 and the “Yee Cell” for both the full grid and half grid [Magic User’s Manual 2007].

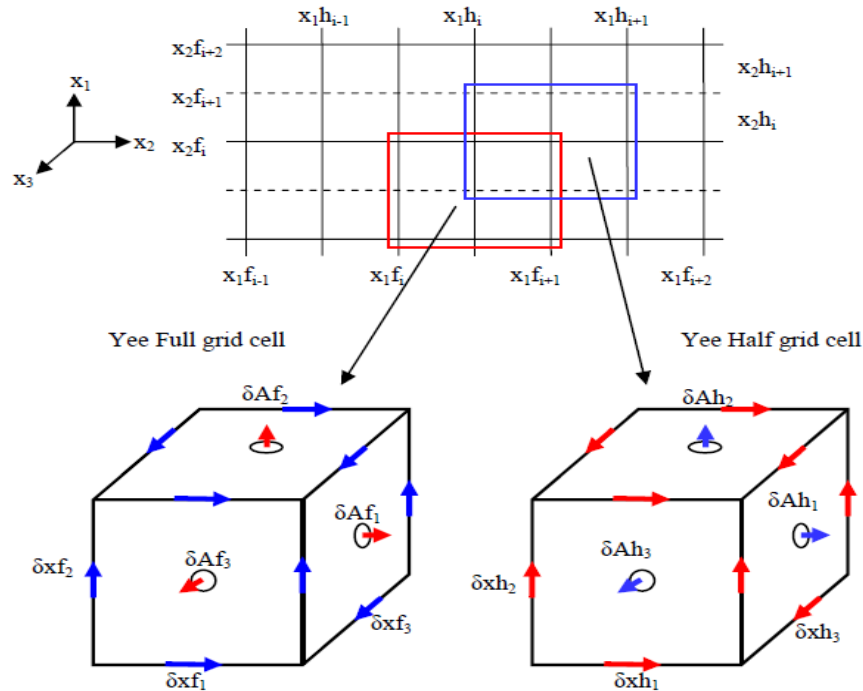


Fig. 3.1 Spatial discretization of simulation space and full grid and half grid assignments of “Yee” cell [Magic User’s Manual 2007].

Finite difference is more robust than any other methods since vector difference equations provide identical properties as vector differential equations. The discretized Maxwell's equations are used to update the fields and are given as:

$$\begin{aligned} [B \cdot dA / dt]^{n+1/2} &= [B \cdot dA / dt]^{n-1/2} - \sum loop [E \cdot dl]^n \\ [D \cdot dA / dt]^{n+1} &= [D \cdot dA / dt]^n + \sum loop [H \cdot dl]^{n+1/2} - [J \cdot dA]^{n+1/2} \\ \sum star [B \cdot dA / dt]^{-1/2} &= 0 \\ \sum star [D \cdot dA / dt]^0 &= [\rho dV / dt]^0 \\ \sum star [J \cdot dA]^{n+1/2} &= [\rho dV / dt]^n - [\rho dV / dt]^{n+1} \end{aligned}$$

The material properties are subsumed in the following equations

$$\begin{aligned} [H \cdot dl]^{n+1/2} &= [dldt / \mu dA][B \cdot dA / dt]^{n+1/2} \\ [E \cdot dl]^n &= [dldt / \epsilon dA][D \cdot dA / dt]^n \end{aligned}$$

where the superscript n represents the discrete time step.

The electric (E) and magnetic (B) fields are updated in time in a leapfrogged manner. Electric (E) fields are solved at integer time steps and magnetic (B) fields are solved on integer plus half time steps and can be easily observed in Fig. 3.2. In addition, the particle variables such as space coordinate, momentum and current (x , p and J) associated with integer or integer+1/2 time steps in a similar manner.

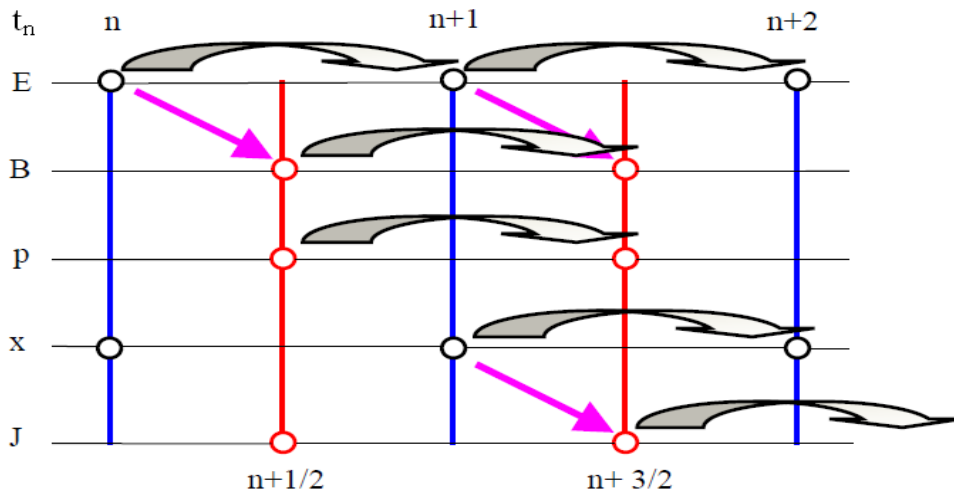


Fig. 3.2 Scheme of update for electric (E) and magnetic (B) fields, space coordinates, momentum and current in simulation [Magic User's Manual 2007].

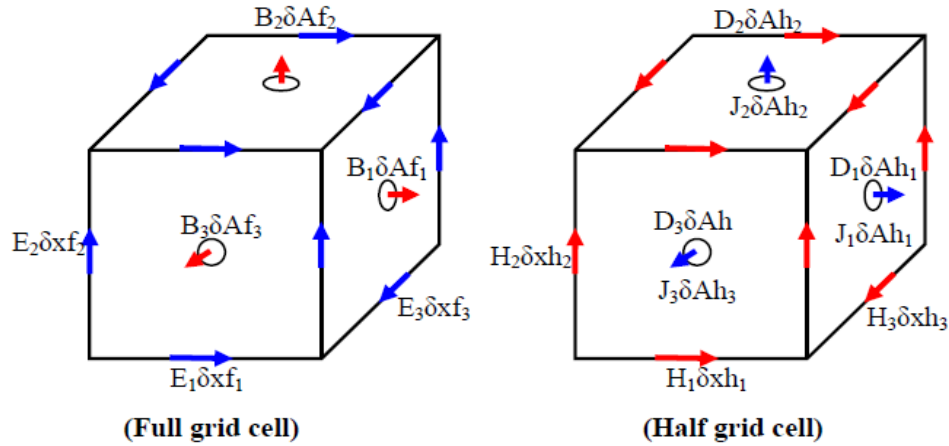


Fig. 3.3 Various fields association in full grid and half grid cell [Magic User's Manual 2007].

The Ampere's law and Faraday's law can be realized on the Yee cell as in following Fig. 3.3. The components of ' J ' have the same "Yee Cell" association as does the electric field components.

3.2.2 PIC Simulation Description

MAGIC Tool Suite is used in a wide range, especially for carrying out simulation of electromagnetic fields interacting with charged particles in 2D/3D. There are several steps required to obtain the solution of beam-wave interaction problems in MAGIC similar to any other PIC codes. Working with this software, requires developing code for problem concern in an editor, so-called Mugman. The flow chart shown in Fig. 3.4 illustrates the order in which to create a MAGIC simulation. This order is designed to allow MAGIC to self-check many conditions that are necessary for simulation reliability.

To start with MAGIC first, identification is needed to provide unique identification (HEADER) for the simulation, and it appears on all simulation output. At the beginning, a coordinate system (SYSTEM) must be chosen properly related to the problem from the available options, i.e., Cartesian, cylindrical, polar, or spherical. The selection will fix the identification of generalized coordinates (e.g., x_1, x_2, x_3) with physical (e.g., x, y, z) coordinates. Variables can be used as data entries anywhere in place of the constants. However, One must assign values to such variables before they are used (ASSIGN) [Magic User's Manual 2007].

MAGIC uses MKSA system of units for input and output. Generalized particle momentum is an exception which omits rest mass from definitions. In general, the correct physical units are stated in the command argument definitions and in printed and plotted output. The constants entered using other units (ASSIGN) will be automatically converted to MKSA values during the simulation process.

One may create arbitrary spatial objects consisting of points, lines, areas, and volumes of diverse shapes (POINT, LINE, AREA, VOLUME). The only attribute of spatial objects is geometric. One must use other commands to assign physical properties to such objects or to use them for some other purpose. To create hollow objects, make two objects of same type with some thickness and then assign the material properties to the outer one, use void for the inner one [Magic User's Manual 2007].

After this, a vital step is to construct a grid in two or three spatial coordinates, i.e., dividing the structure into cells, using either automatic or manual gridding. To use automatic gridding, one must mark at least some of the spatial objects (MARK). To use manual gridding, One must specify the grid origin (GRID ORIGIN) followed by arbitrary regions of grid. The spatial grid is the primary determinant of accuracy (the time step is generally unimportant to accuracy), and all spatial phenomena of interest must be appropriately resolved. Time period must be defined using DURATION command in simulation for the desired time duration to be covered.

Next step is to define the field algorithm, it may be either MAXWELL HIGH_Q, MAXWELL CENTERED. One may replace the default electromagnetic field algorithm (MAXWELL) and specify the time step (TIME_STEP). Depending on an algorithm, the number of particles emitted from the cathode will be different. The default field algorithms are suitable for mildly relativistic particle simulations, e.g., γ up to 1.5. The time step, spatial grid, and algorithm are the primary determinants of numerical stability. If the time step exceeds the Courant criterion, unambiguous catastrophic failure results obtained. Highly relativistic particle simulations produce more noise, and numerical

damping of this noise is another important property, which depends on the choice of the electromagnetic algorithm.

Physical properties should be assigned to spatial objects such as infinite conductivity, permittivity, etc., only to spatial areas (2D simulations) or volumes (3D simulations). Unique structural properties, such as the inductive strut, can be assigned merely to spatial line. A point cannot assign a physical property.

Assign outer boundary properties to spatial objects on the simulation perimeter. The perimeter shape and location are arbitrary. Most outer boundaries (SYMMETRY, PORT, OUTGOING) etc., can be applied only to spatial lines (2D simulations) or areas (3D simulations). One exception (FREESPACE) applies only to spatial areas (2D) or volumes (3D).

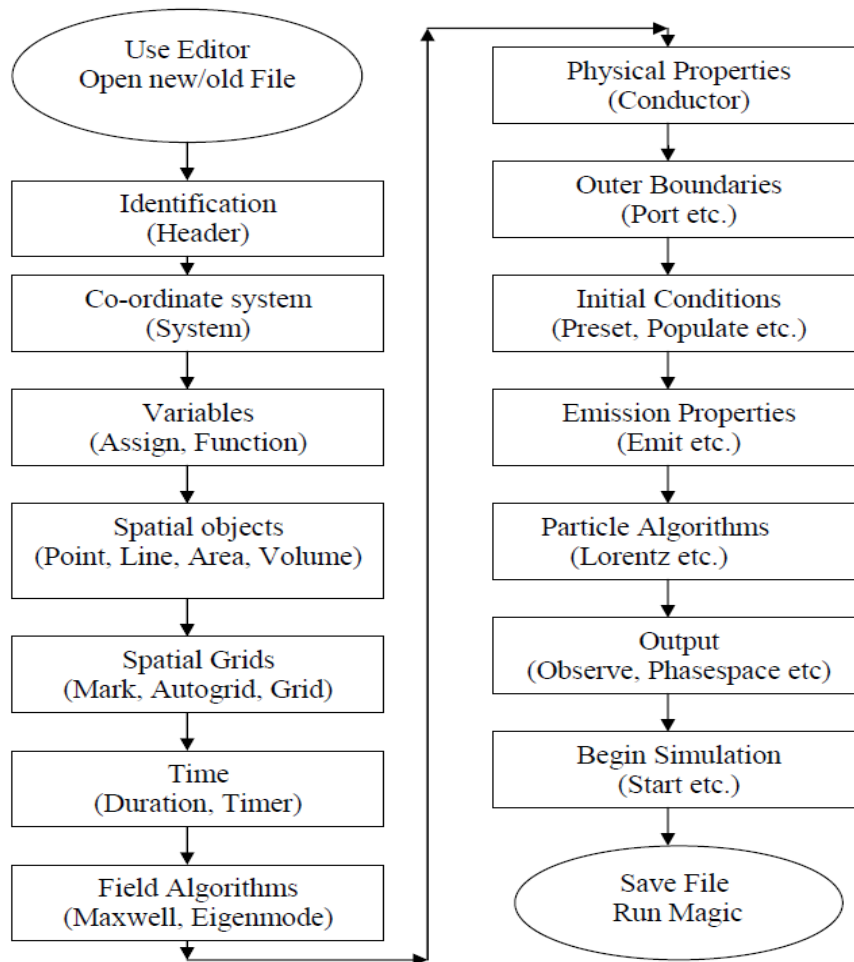


Fig. 3.4 Flow chart illustrating the order in which the simulation is created [Magic User's Manual 2007].

Assign emission properties to the cathode surface, by using EMISSION command. The EMIT command enables emission from the specific object we have selected, i.e., cathode. Specify explicitly output required (various commands) and timer is used to trigger output at different times during the simulation (TIMER).

Most simulations start from trivial initial conditions without fields or particles. However, non-trivial initial conditions may be supplied explicitly by creating initial magnetic fields (PRESET) and particles (POPULATE).

External current density is introduced by using CURRENT_SOURCE, DRIVER commands. The DRIVER command specifies a prescribed (analytic) current-density source to drive electromagnetic fields in a local region of space. The DRIVER is used wherever it makes sense physically to excite the modes of interest. The DRIVER should always be entirely within the simulation boundaries [Magic User's Manual 2007].

One must explicitly specify any output required (various commands). A timer is used to trigger output at different times during the simulation. Finally, one must terminate the input file to execute the simulation (START) or to stop processing (STOP).

3.3 PIC Simulation of a Two-Cavity Gyroklystron Amplifier

The process of designing a gyroklystron includes the choice of the RF operating mode corresponding to the RF interaction structure, electron beam parameter, and magnetic field. The finalization of the RF interaction structure consists of several steps. First, the resonance frequency and quality factor with a desired field profile for each of the cavities are chosen. Based on this information, cavities shape, size and connecting drift tube radii are selected. To ascertain this, electromagnetic analysis of gyroklystron structure is carried out in the absence of the electron beam, also known as the cold analysis. The results obtained from the cold analysis are used to predict the electron beam and RF wave interaction behavior of the gyroklystron device in the presence of the electron beam which is simply known as the hot analysis. At this point, the various device input

parameters, such as, beam current, voltage, transverse to axial beam velocity ratio (pitch factor), guiding center radius and magnetic field values are judiciously chosen with the help of its parametric analysis. The operating current and the magnetic field are mainly decided by the start oscillation current criteria study, necessary for the stable operation of the device. The coupling coefficient curve helps us to launch the electron beam at optimum beam radius for maximum beam to mode coupling.

3.3.1 RF interaction structure modeling

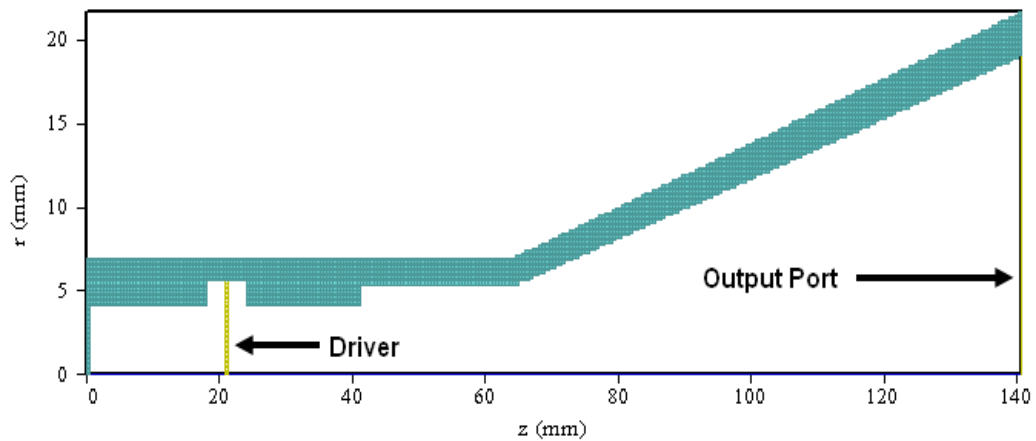


Fig. 3.5 Cross-section of the two-cavity gyroklystron interaction structure.

A three-dimensional structure consisting of all-metal cylindrical cavities, is modeled using the cylindrical coordinate system (z, r, θ) for PIC simulation using ‘MAGIC’ code. Material properties of the cavities walls are typically assigned as metal (copper). The conductivity of the copper used in the simulation is taken as 5.8×10^7 S/m. A port has been assigned at the output taper end to observe the output signal. The cross-sectional view of the model used in the PIC simulation is shown in Fig. 3.5. Proper meshing is made for the discretization of the structure to get fast converging results. External loading in the RF input cavity is done to achieve the desired quality factor by observing the EM energy decay inside the cavity. Drift tube is externally loaded to avoid any cross-talk between the two cavities by absorbing the field leaked from the cavities. In ‘MAGIC’ software CONDUCTANCE command is used to define the lossy material. The CONDUCTANCE command specifies a finite conductivity (mhos/m) within an

object. It must be a volume in a 3D simulation. The conductance may be entered by specifying the conductivity of the material. Conductivity will be applied only within the specified object and will result in an additional current as specified by Ohm's Law, $\mathbf{J} = \sigma \mathbf{E}$, which is applied to Ampere's law as an additional current source. The ohmic power dissipated due to this conductance material allows us to achieve the desired quality factor [Magic user's Manual (2007)]. In our simulation, we have used the conductance of material = 0.01 mhos/m for loading the input cavity. The conductance of material = 0.04 mhos/m has been taken for loading the drift tube.

The gyrating electron beam of desired guiding center radius is introduced at the input end of the interaction structure with the help of gyro beam emission command of this PIC code. The gyro emission produces a beam center axis parallel to the externally applied magnetic field. The external static magnetic field of strength 1.31 T is applied axially along the interaction structure. The typically selected design parameters for the present work are taken from the reported experimental results of J. J. Choi [Choi *et al.* (1998)]. The RF input and output cavities lengths for the present gyroklystron are taken as $1.5\lambda = 12.85$ mm and $2.75\lambda = 23.56$ mm, respectively, for the operating TE_{01} mode resonating at 35 GHz [Choi *et al.* (1998)]. The length of the RF output cavity is taken larger than that of the input cavity to enhance the electron beam and RF wave interaction process in the output cavity to get the maximum RF output power and efficiency. The input and output cavity radii are 5.6 mm and 5.35 mm, respectively. The drift tube is in cutoff to the operating mode with length equal to $1.7\lambda = 14.57$ mm, and radius equal to 4.1 mm. The present gyroklystron utilizes a gyrating electron beam of 70 kV, 8.2 A having the velocity pitch factor of 1.43 and beam radius equal to 2.65 mm.

3.3.2 Eigenmode and electromagnetic fields

Electromagnetic simulation of the gyroklystron cavities has been carried out before the PIC simulation to observe the desired operating mode and resonant frequency in the absence of the beam using eigenmode analysis. Using this technique, the presence of a particular mode inside the cavities is confirmed by

observing the electric field pattern. Fig. 3.6 shows the vector and contour plots of electric field, respectively, of the input cavity of the gyroklystron which indicates that the desired TE_{01} mode is present inside the cavity.

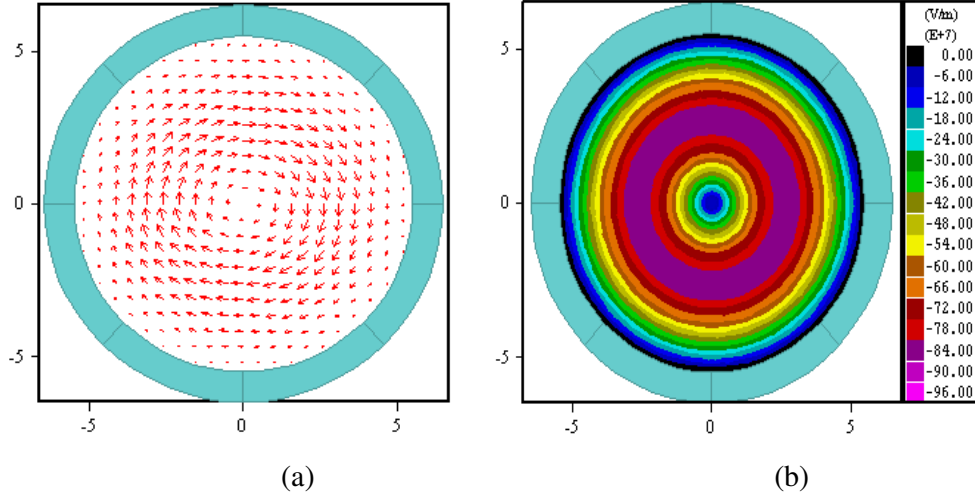


Fig. 3.6 Electric field (a) vector plot, and (b) contour plot for input cavity of gyroklystron.

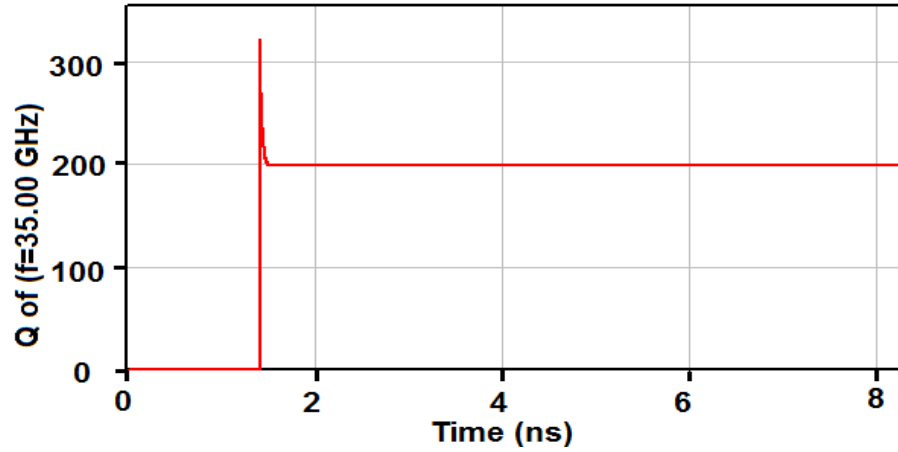


Fig. 3.7 Quality factor for input cavity of gyroklystron.

The overall quality factor of a cavity can be obtained using well known relation, $(Q_{total})^{-1} = (1/Q_{ohmic})^{-1} + (1/Q_{diffractive})^{-1}$. The diffractive quality factor for a closed cavity is usually very high. Therefore, the total quality factor of the cavity is approximately equal to the ohmic quality factor. The gyroklystron cavity is loaded with lossy ceramics to achieve the desired quality factor.

In the present work, the loaded quality factor of the cavity is optimized to the desired value through external loading. For the estimation of the loaded

quality factor, entire cavity volume is excited by a current driver placed at its center with excitation frequency 35 GHz. The decay of EM energy in the cavity is observed for the estimation of the loaded quality factor. The EM energy decays slowly inside this cavity, which demonstrates the resonant behavior of the interaction structure. For our present simulation, loaded quality factor is obtained ~200. In Fig. 3.7, the required quality factor for the input cavity has been obtained.

3.3.3 Electron beam and RF wave interaction

The hot analysis of gyroklystron is demonstrated by introducing the gyrating electron beam with a beam current of 8.2 A and beam voltage of 70 kV at the left end of the interaction structure. The guiding center radius used here is 2.65 mm. The velocity spread effects are assumed to be zero for carrying out the present simulation. Since, provision for the inclusion of velocity spread effects is not available with PIC code 'MAGIC'. In experimental devices, 5% to 10% velocity spread is usually present, which deteriorates the electron bunching due to degradation in the quality of the electron beam as a result of which both output power and efficiency of the device decrease [Tran. *et al.* (1986)]. Here, eight beamlets are considered to perform the present simulation.

Fig. 3.8(a) shows the cross sections of electron beamlets before interaction and Fig. 3.8(b) shows the cross sections of electron beamlets at the RF output port after the interaction time of 200 ns. The phase of all particles observed in each beamlets, confirm that all beamlets have a constant phase relationship with each other. Fig. 3.9 shows the time variation of electric field amplitude developed at the RF output cavity. The frequency of operation is validated by observing the Fourier transform of the azimuthal electric field component of the time growing signal at the RF input and output cavity. Fig. 3.10 shows the obtained frequency spectrum at the output cavity, characterized by single frequency component, peaked at 34.95 GHz, which validates the frequency and mode of operation in our case. The other noticeable peak of the electric field amplitude is found to be at around 70 GHz, which is corresponding to the second harmonic of electron cyclotron frequency. It is clear from Fig. 3.10 the amplitude difference between

the fundamental harmonic and second harmonic peaks is good enough (~ 32 dB) to ensure that there will be no mode competition.

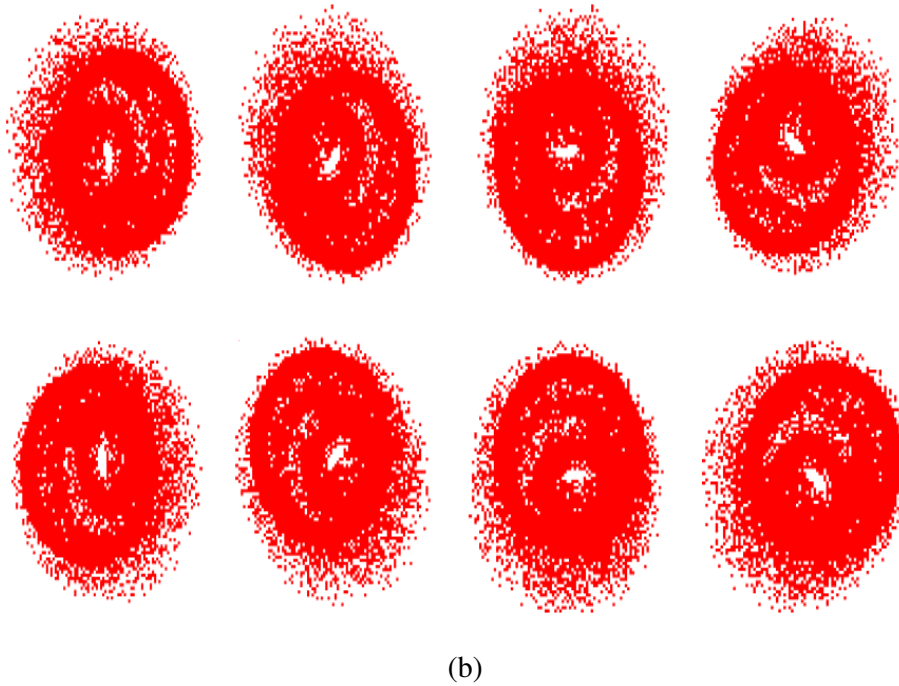
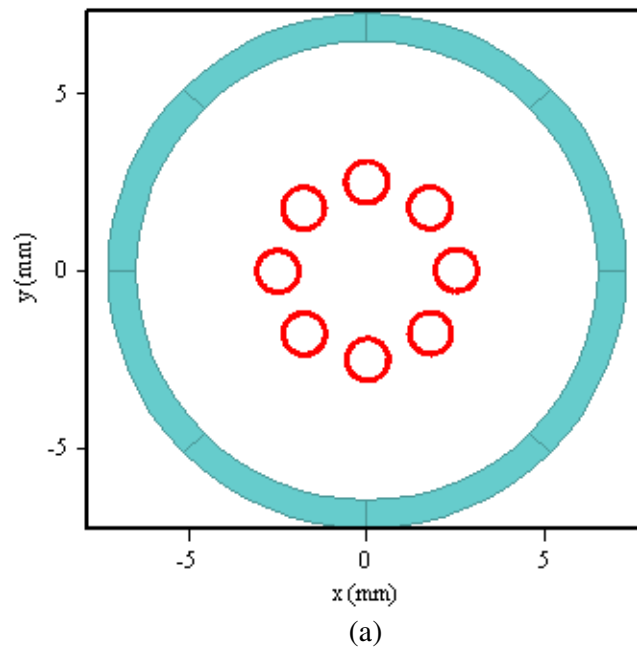


Fig. 3.8 Phase space of electron beamlets (a) before interaction, and (b) after interaction.

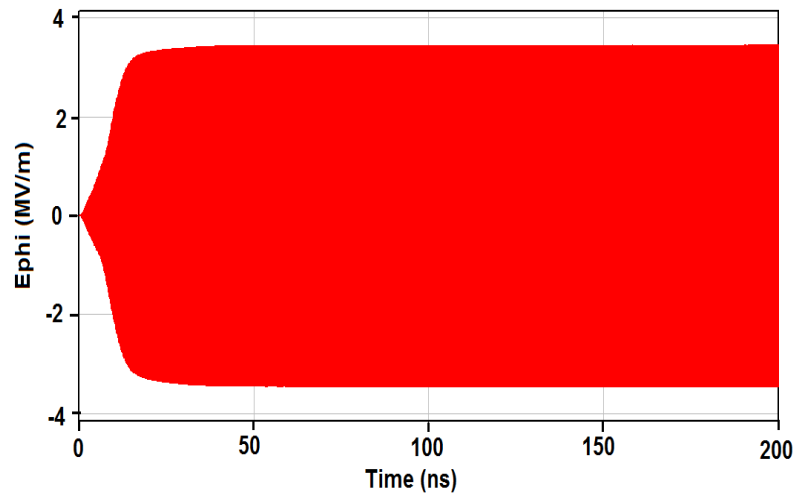


Fig. 3.9 Temporal field magnitude recorded using probe at the output cavity.

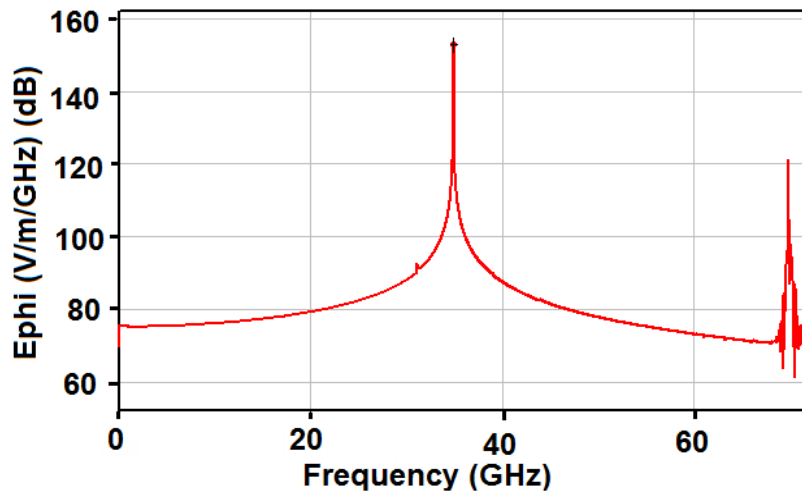


Fig. 3.10 Observed frequency spectrum of the electric field at the output cavity.

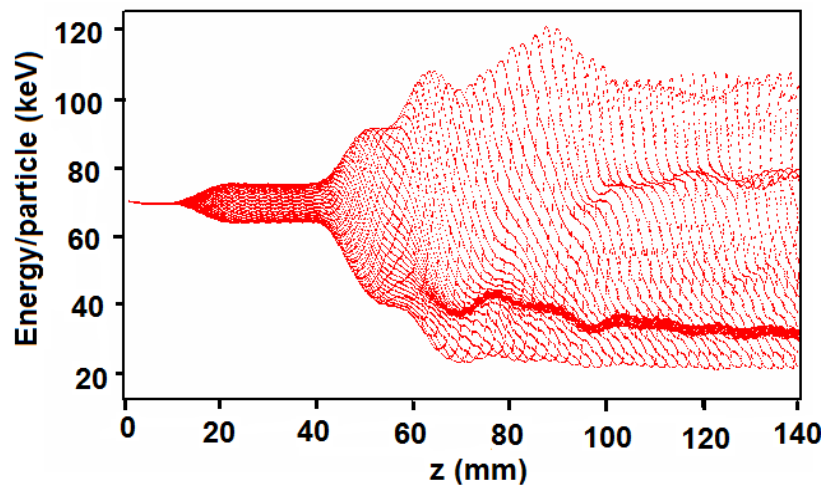


Fig. 3.11 Evolution of particles energy along the interaction length.

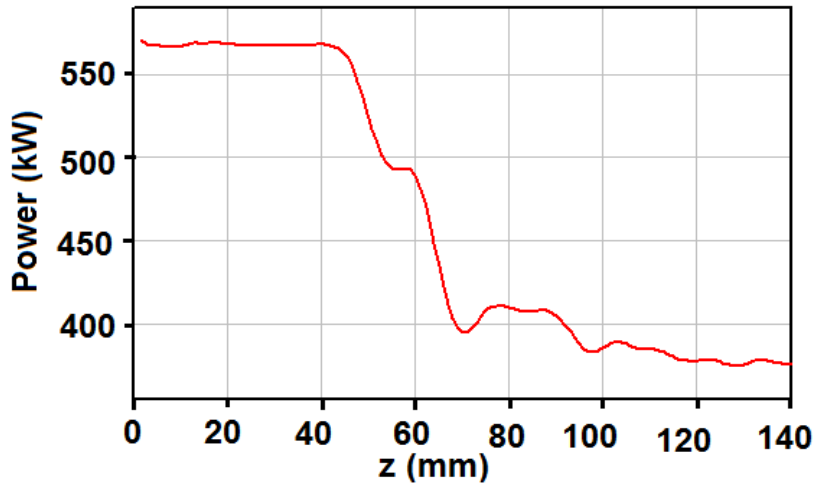


Fig. 3.12 Axial variation of electron positive power.

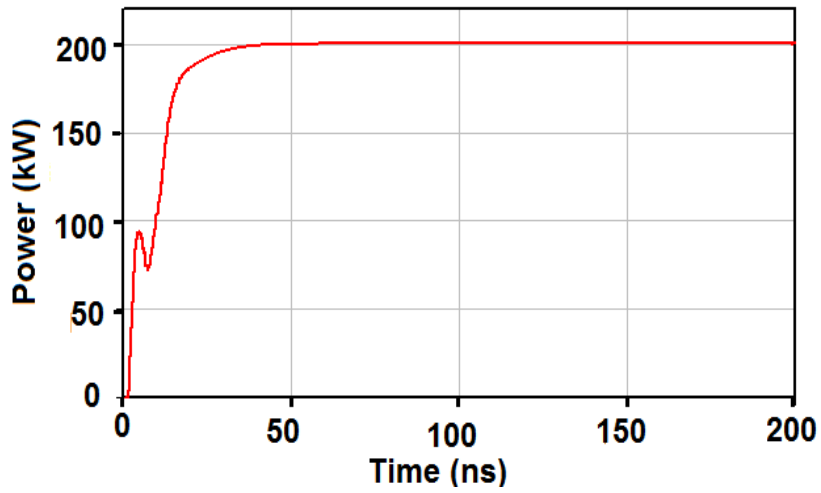


Fig. 3.13 RF output power.

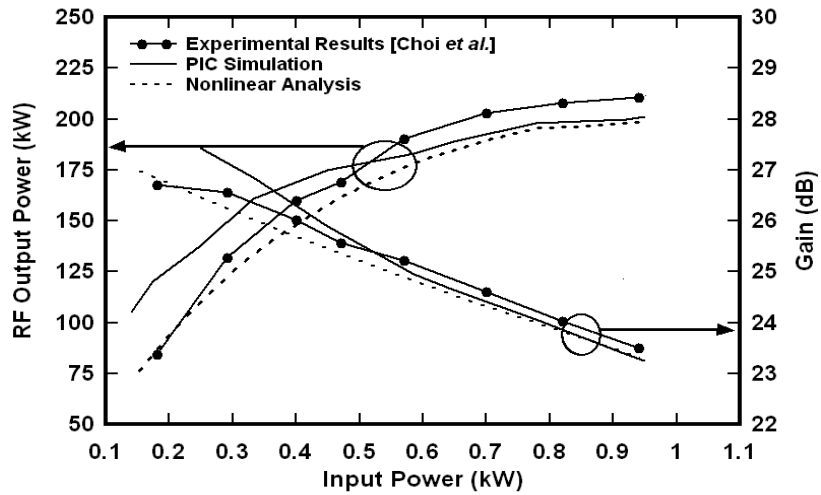


Fig. 3.14 RF output power and gain as a function of the input power.

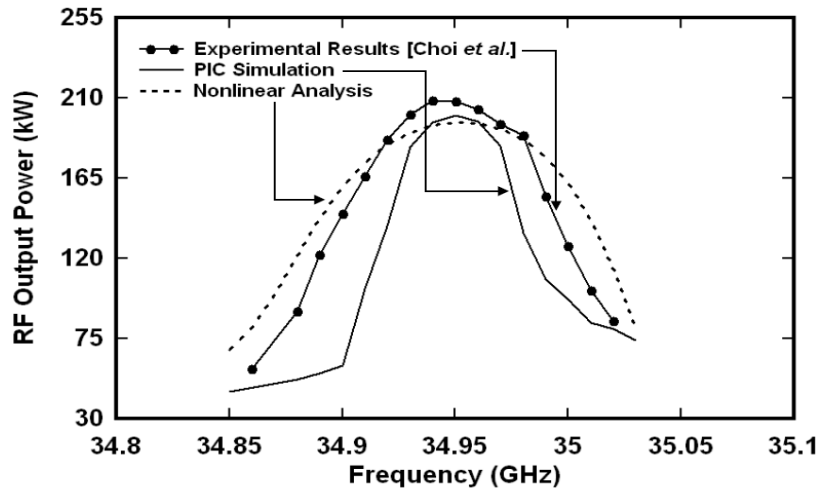


Fig. 3.15 Output power as a function of drive frequency.

Figures 3.11 and 3.12 show the evolution of electronic energy and power along axes, respectively. It can be seen that at the output end, the net electron energy and power are decreasing, indicating an energy transfer from the electrons to the RF wave. The RF input signal is applied to the input cavity with the help of an input driver. The DRIVER command specifies a prescribed current-density source to drive electromagnetic fields in a local region of space. The desired mode corresponding to specific frequency and power can be excited with the help of this command. The power developed across this driver serves as the RF input power for our device. In our simulation, the RF input power is ~ 922 W. The growth rate of RF output power with time is shown in Fig. 3.13. The radiated power of 200 kW reaches to saturation value at 40 ns, corresponding to power conversion efficiency of 35% where beam voltage is 70 kV and beam current is 8.2 A. The variation of RF output power and gain achieved as a function of input power using MAGIC code has been shown in Fig. 3.14. The 3 dB bandwidth calculation of the device is done by plotting the output power and efficiency as a function of frequency (Fig. 3.15). The 3 dB bandwidth obtained for this device is 0.29% (100 MHz). The simulated results obtained here are compared for the validation purpose with the experimental results of Choi *et al.* and large signal analysis results obtained in previous chapter, Chapter 2 (Figs. 3.14 and 3.15) [Choi *et al.* (1998)]. The present PIC results are in agreement with the experimental values as well as with those predicted by the large signal analytical model of the

gyroklystron. The saturated output power, gain and bandwidth predications obtained from the PIC simulation are found matching with the analytical model along with the experimental results within $\pm 5\%$.

3.4 PIC Simulation of a Four-Cavity Gyroklystron Amplifier

In order to enhance the bunching process in a gyroklystron amplifier the more number of cavities are added to the RF interaction structure. The main advantage of a multicavity gyroklystron amplifier over the basic two-cavity gyroklystron model is the enhancement in the gain of the device. Also, the performance improvement technique, like, stagger tuning can be effectively implemented on a multicavity gyroklystron as compared to two-cavity gyroklystron. Keeping these aspects in view, the PIC simulation of a Ka-band, four-cavity gyroklystron amplifier is implemented. In order to study the beam-wave interaction mechanism in the four-cavity gyroklystron amplifier, firstly, the structure is simulated in the beam absent (cold) case to ensure the cavity operation in the desired mode and frequency and followed by the beam present (hot) case is executed. The relevant design parameters for the typical selected 35 GHz gyroklystron amplifier have been listed in Table 2.2. In the beam present case, a gyrating electron beam of 72 keV energy and transverse-to-axial velocity ratio (α) = 1.36 is introduced at the input end of the input cavity with a beam radius of 2.65 mm.

3.4.1 RF Interaction structure modeling

A three-dimensional RF structure of a four-cavity gyroklystron has been modeled using the three-dimensional version of the MAGIC code. The cross-sectional view of the model used for the PIC simulation is illustrated in Fig. 3.16. The coordinate system used here for modeling the structure in MAGIC is the cylindrical coordinate system (z, r, θ). As shown in Fig. 3.16, the present gyroklystron consists of four cylindrical cavities with input cavity length equal to 12.85 mm, input cavity radius equal to 5.6 mm, second and third cavities lengths are equal to 14.56 mm and radius equal to 5.5 mm. The output cavity has a length 23.58 mm and radius 5.34 mm. The cavities are isolated to each other with the

help of drift tubes, which are cutoff to the operating mode. The drift tube has a radius 4.1 mm and length 14.56 mm. The cavities are externally loaded to achieve the desired quality factor. Drift tubes are externally loaded to avoid any cross-talk between the two cavities by absorbing the field leaked from cavities to drift region [Garven *et al.* (2000)].

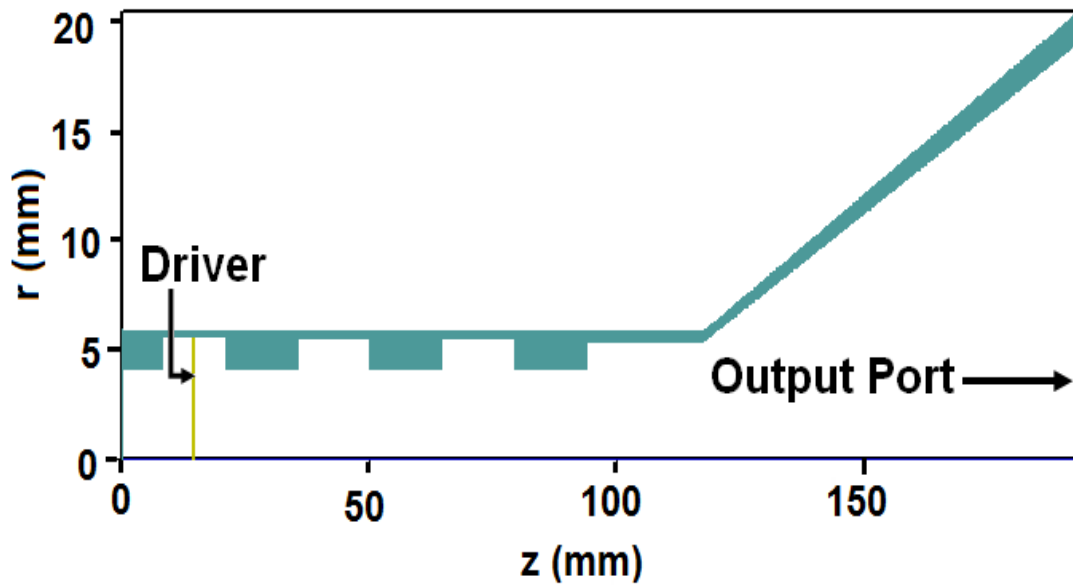


Fig. 3.16 Cross-section of a four-cavity gyroklystron interaction structure.

3.4.2 Eigenmode and electromagnetic fields

The cold cavity simulation of all the cavities of the gyroklystron amplifier is performed using EIGENMODE command of the MAGIC code, specifies an eigenvalue solution of the fully time-dependent Maxwell's equations. Fields at corresponding frequency can be observed. If nothing is specified it will give us the dominant mode of the structure. The software doesn't display the specification of the modes. So, the different TE and TM modes are identified by observing the field patterns. The field patterns on different planes of interest as well as field profile along radial and axial positions can be observed to ensure the desired mode. The electric field vector and contour patterns in the mid plane of input cavity are shown in Fig. 3.17. Clearly, vector and contour plots of electric field ensure the

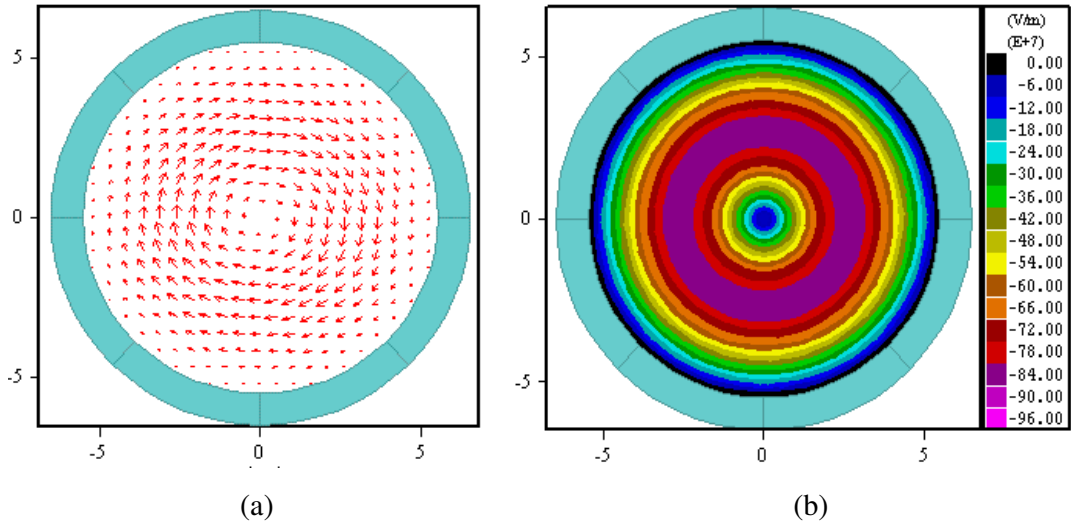


Fig. 3.17 Electric field (a) vector plot, and (b) contour plot for input cavity of four-cavity gyrokystron.

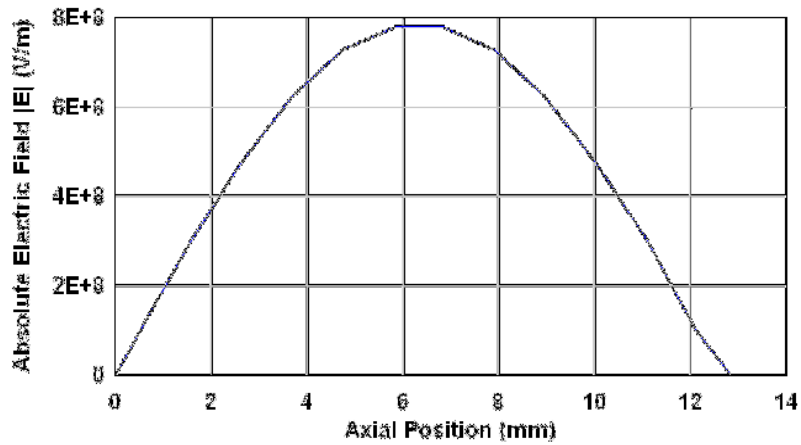


Fig. 3.18 Variation of electric field magnitude along axial direction of input cavity.

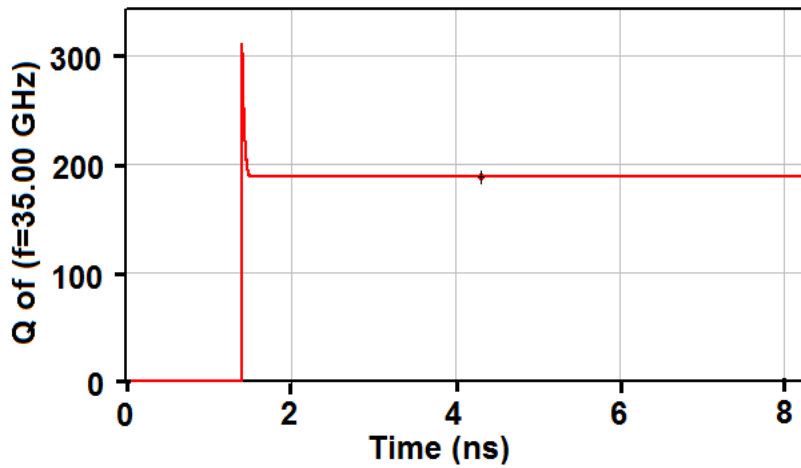


Fig. 3.19 Quality factor for input cavity of four-cavity gyrokystron.

TE_{01} mode at 35 GHz resonant frequencies with magnitude as well as orientation. The axial variation of the electric field magnitude is shown in Fig. 3.18. The axial pattern of electric field shown in Fig. 3.18, shows that the field is maximum in the middle of the cavity which is necessary for strong beam wave interaction process.

The next step in the cold cavity simulation process is the estimation of the desired quality factor of the cavity. As, the performance of a gyroklystron amplifier is very much dependent on the quality factor of its individual cavities. Therefore, the estimation of the desired quality factor of each cavity before hot simulation is necessary, because it is difficult to predict the correct value of the quality factor in the presence of the electron beam. The loaded quality factor (Q) of the cavity has been calculated by exciting the entire cavity volume by a current driver placed at its center with excitation frequency 35 GHz and calculating the decay of electromagnetic energy inside the cavity. For the present gyroklystron amplifier, the desired quality factor for input cavity is 188. In Fig. 3.19, desired quality factor equal to 188 has been obtained for the input cavity.

3.4.3 Electron beam and RF wave interaction

After the cold cavity simulation, the beam-wave interaction simulation is carried out for the performance estimations of the gyroklystron amplifier, i.e., output power, efficiency, gain, bandwidth, etc., in the presence of a gyrating electron beam. For this purpose, a gyrating electron beam is launched at the entrance of the input cavity of the four-cavity gyroklystron amplifier. After interacting with the TE mode of the input cavity which is excited with the help of a driver, the gyrating electron beam drifts through intermediate cavities and drift tubes of the RF section of the gyroklystron amplifier. As the electrons drift through the input cavity, in-between cavities and drift tubes a kind of bunching (called azimuthal or phase bunching) occurs in the electron beam due to this a center of the bunch is formed at the inlet of the output cavity. In the output cavity, these bunched electrons lose their energy to the RF and disperse in the phase space with reduced Larmor radii towards the outlet of the output cavity. Figure 3.20 clearly indicates the loss in kinetic energy of the electrons and also the density of the electrons varies with the axial length of the RF interaction structure of the

gyroklystron amplifier. Most of the electrons are below the energy of 72 keV (indicated by thick black line), and this indicates the electron beam energy transfer from the electrons to the RF. Figure 3.21 shows the variation in electron positive power along the interaction length. It can be seen from Fig. 3.21 that around 190 kW of electron beam power is lost by the electrons during the beam wave interaction process.

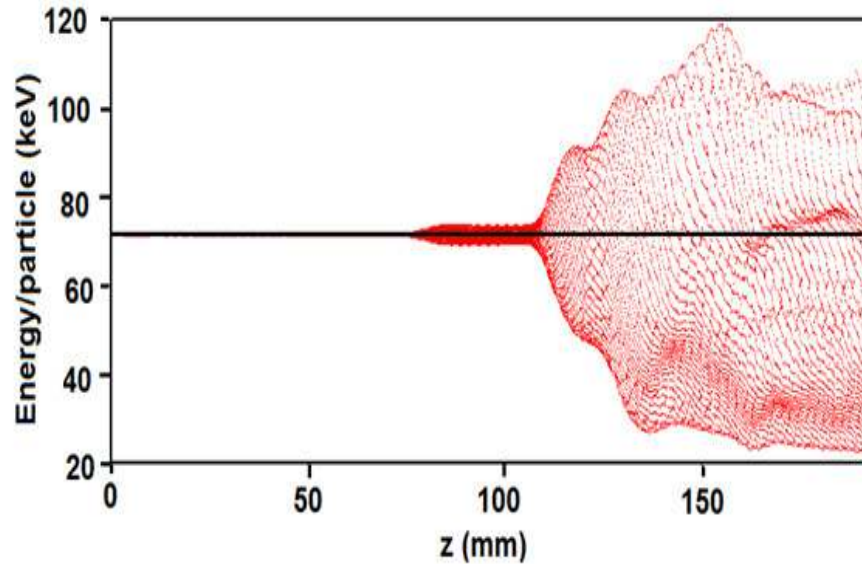


Fig. 3.20 Energy distribution of all the electrons along the interaction length.

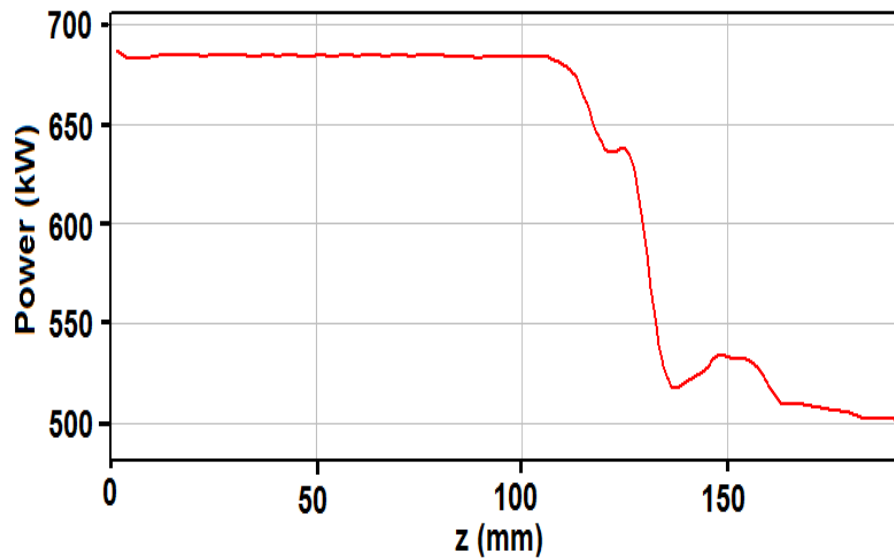


Fig. 3.21 Variation in electron positive power along the axis of interaction structure.

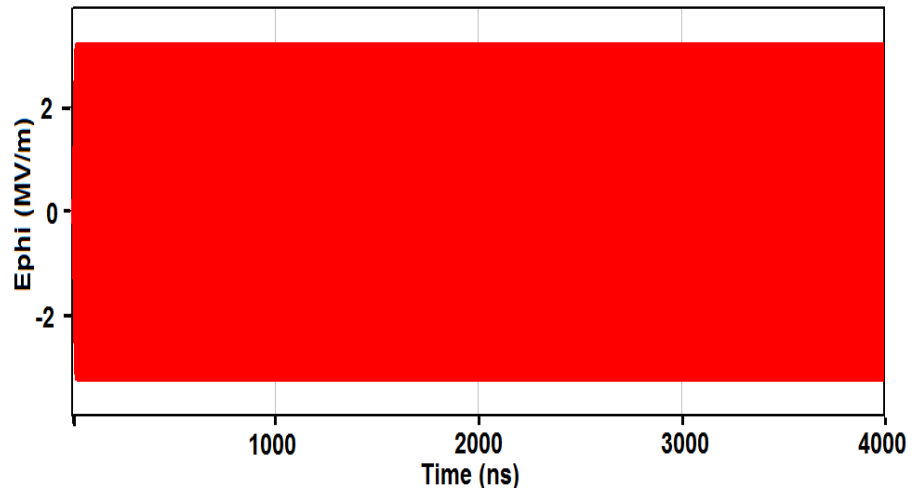


Fig. 3.22 Growth of the electric field amplitude with respect to time at the output cavity.

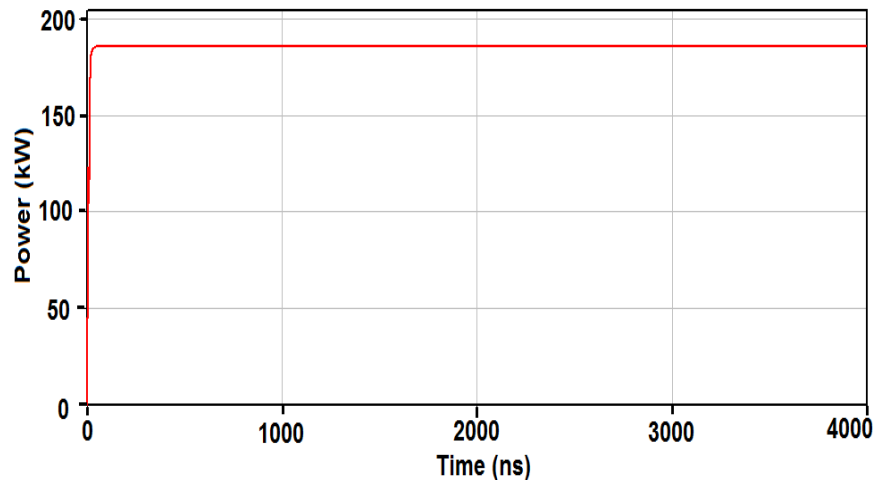


Fig. 3.23 Temporal growth of RF output power.

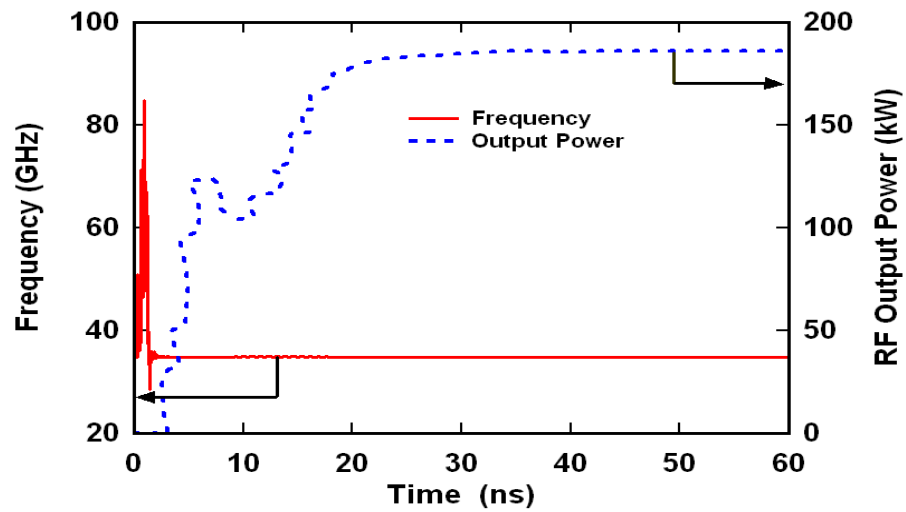


Fig. 3.24 Frequency and power growth with respect to time.

Figures 3.22 and 3.23 show the growths of electric field and power with respect to time. These typical diagrams represent the time history of the beam-wave interaction process. In Fig. 3.22 the electric field growth is recorded for a time duration of 4000 ns. It is clear from Fig. 3.22 that the field amplitude becomes stable after 30 ns and after that remains steady during the whole interaction process. In Fig. 3.23, the temporal growth of RF output power corresponding to 0.43 W RF input power is observed. The RF output power gets to steady state at around 185 kW after 30 ns, corresponding to power conversion efficiency of 26.7% and after that remains stable for the entire duration of simulation runtime, i.e., 4000 ns. Figure 3.24 shows the typical plots of MAGIC simulation representing the frequency and power growth with respect to time in the output cavity. These two figures simply give an idea about the frequency and power growths occur in the preferred mode of a gyroklystron amplifier. In Fig. 3.24, first the frequency gets stable to 34.90 GHz around 3 ns second indicating towards the setup of the desired TE_{01} mode in the output cavity. After that, the stability in output power of the operating TE mode (185 kW) is achieved around 30 ns.

Figure 3.25 is a frequency spectrum curve of the output cavity. The curve shows the gain in the RF signals of the different frequencies in the output cavity. The curve is found through Fast Fourier Transform (FFT) of the time history of the electric field amplitude plot shown in Fig. 3.22. It is a very important curve, which gives information about the signal growth of the desired mode and the competing mode. The sharp peak in Fig. 3.25 is corresponding to the frequency of 34.90 GHz and confirms the excitation of desired TE_{01} mode because the calculated resonant frequency (f_r) of this mode, obtained from the eigenmode simulation (cold cavity simulation) of the output cavity is nearly equal. Surrounding the peak of 34.90 GHz, the nearest peak is at frequency 69.80 GHz corresponding to the second harmonic operation of the gyroklystron amplifier. The 69.80 GHz electric field peak has lower amplitude almost 42 dB less with respect to 34.90 GHz electric field peak (Fig. 3.25) and thus the TE mode corresponding to second harmonic at 69.80 GHz is unable to create competition

with the operating TE_{01} mode at 34.90 GHz. The excitation of desired TE_{01} is also confirmed by the Fig. 3.24 which shows the temporal growth of frequency and power corresponding to this mode.

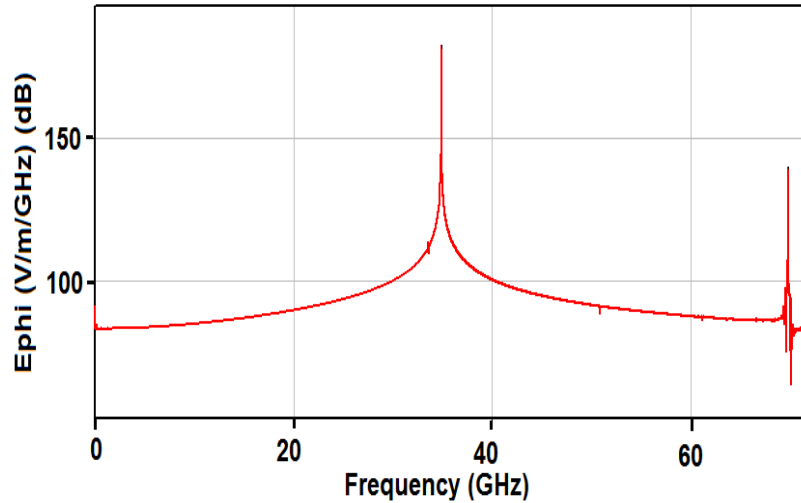


Fig. 3.25 Frequency spectrum of the output cavity.

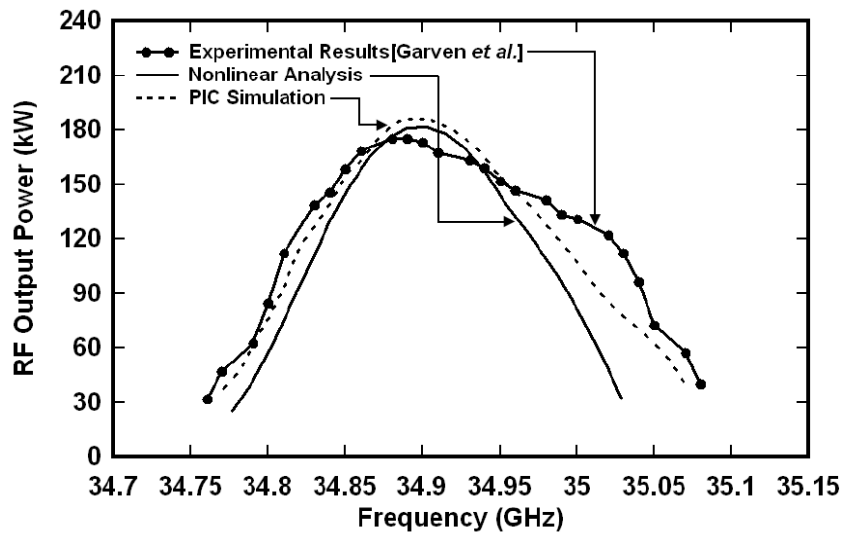


Fig. 3.26 RF output power as a function of drive frequency.

Figure 3.26, shows the comparison of the reported experimental results with the simulated and analytically obtained results for the variation of output power with drive frequency. It is clear from Fig. 3.26 that the present gyrokystron amplifier achieved 185 kW peak output power at center frequency 34.9 GHz with a -3 dB bandwidth of 0.61% (214 MHz). It can be seen from the Fig. 3.26, the

analytical and simulated results obtained here are in good agreement with the reported experimental results within $\pm 5\%$.

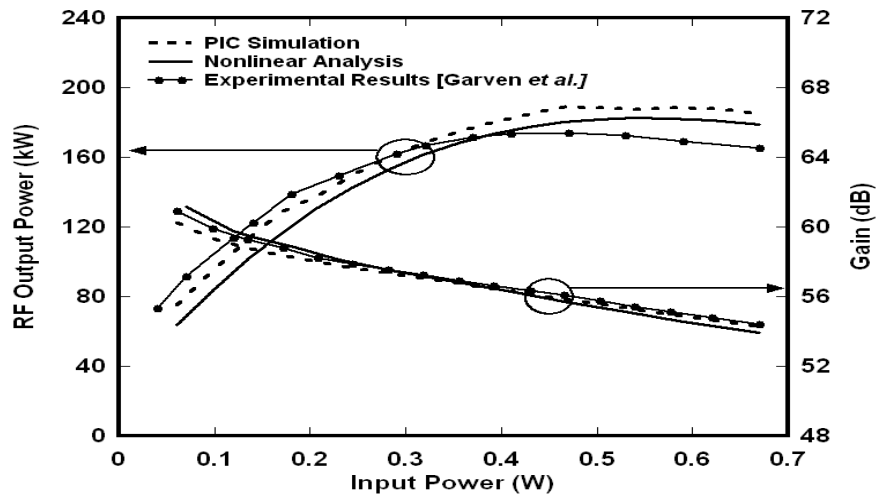


Fig. 3.27 Output power and gain as a function of the input power.

Figure 3.27 shows the peak output power and gain as a function of input power. As seen from figure, the output power reaches saturated value of 180 kW at 0.43 W drive power corresponding to 56 dB gain in case of nonlinear theory and 185 kW corresponding to 56.3 dB gain obtained through the PIC simulation. The results obtained from nonlinear analysis and PIC simulation are in agreement with the reported experimental results within $\sim 5\%$.

3.5 Conclusion

PIC simulation has proved as an important tool to explore the device behavior. It supplements the analytical results as well as reduces the development time. Gyroklystrons have also been investigated through PIC simulations but mostly in-house custom built codes were used which are not available in public domain. Also, detailed investigation of PIC results are not reported in the literature. In the present work reported in this chapter, Chapter 3, a commercially available particle-in-cell code 'MAGIC' has been used for 3D simulation of gyroklystron amplifier. 3D PIC simulation has been performed both for the beam absent and beam present cases using this commercial code. The simulation

procedure and beam-wave interaction investigation have been thoroughly described.

Firstly, the RF cavity simulation has been performed in the beam absent case to examine the cavity operating mode, frequency as well as electric and magnetic field profile. Electric field patterns obtained through simulation confirms the device operation in the desired mode. After the cold cavity simulation the beam-wave interaction analysis has been carried out for the estimations of the RF output performance of the device in the presence of the electron beam (hot condition).

To establish the PIC simulation procedure of a gyroklystron amplifier conventional, cylindrical two-cavity and four-cavity Ka-band (35 GHz) operating in the TE_{01} mode experimental gyroklystron amplifiers reported in the literature have been selected and 3D simulated for its beam-wave interaction behaviour. Further, the loaded quality factor of each cavity is optimized to the desired value through external dielectric loading. Electron beamlets observed at the output port at the end of simulation shows the bunching mechanism of the particles. The energy distribution of all the electrons along the interaction length confirm the net energy transfer from beam to RF. Electric field patterns have been also observed during the whole simulation run time, which confirm the operation in the desired TE_{01} mode during the beam-wave interaction process. In addition to this, parametric analyses have been also carried out with respect to changes in input power and frequency to study the influence of these parameters on output power and to estimate the gain and bandwidth of the device. In the end, the gyroklystron amplifiers simulation results have been compared with the analytical results obtained in Chapter 2 and with the reported experimental results available in the literature. The simulated values have been found in agreement with the analytical results and published experimental results within $\sim 5\%$.